

Anisotropic superconducting properties of aligned $\text{Sm}_{0.95}\text{La}_{0.05}\text{FeAsO}_{0.85}\text{F}_{0.15}$ microcrystalline powder

B. C. Chang¹, C. H. Hsu¹, Y. Y. Hsu², Z. Wei³, K. Q. Ruan³, X. G. Li³, and H. C. Ku^{1*}

¹Department of Physics, National Tsing Hua University, Hsinchu 30013, Taiwan

²Department of Physics, National Taiwan Normal University, Taipei 10610, Taiwan

³Hefei National Laboratory for Physical Sciences at Microscale and Department of Physics, University of Science and Technology of China, Hefei 230026, China

(Dated: July 17, 2008)

The $\text{Sm}_{0.95}\text{La}_{0.05}\text{FeAsO}_{0.85}\text{F}_{0.15}$ compound is a quasi-2D layered superconductor with a superconducting transition temperature $T_c = 52$ K. Due to the Fe spin-orbital related anisotropic exchange coupling (antiferromagnetic or ferromagnetic fluctuation), the tetragonal microcrystalline powder can be aligned at room temperature using the field-rotation method where the tetragonal ab -plane is parallel to the aligned magnetic field B_a and c -axis along the rotation axis. Anisotropic superconducting properties with anisotropic diamagnetic ratio $\chi_c/\chi_{ab} \sim 2.4 + 0.6$ was observed from low field susceptibility $\chi(T)$ and magnetization $M(B_a)$. The anisotropic low-field phase diagram with the variation of lower critical field gives a zero-temperature penetration depth $\lambda_c(0) = 280$ nm and $\lambda_{ab}(0) = 120$ nm. The magnetic fluctuation used for powder alignment at 300 K may be related with the pairing mechanism of superconductivity at lower temperature.

PACS numbers: 74.72.-h, 74.25.Ha

High- T_c superconductivity with transition temperature T_c up to 55 K were reported in the newly discovered iron-based $\text{RFeAsO}_{1-x}\text{F}_x$ (rare earth $R = \text{La, Ce, Pr, Nd or Sm}$) system [1, 2, 3, 4, 5, 6, 7, 8, 9, 10, 11, 12]. The ZrCuAsSi -type tetragonal structure (space group $P4/nmm$) is a layered structure where the metallic FeAs layer is separated by the insulating $\text{RO}_{1-x}\text{F}_x$ layer. The discovery of the iron-based superconductor has generated enormous interest since these compounds are the first non-cuprate high- T_c superconductors with T_c higher than 50 K. The parent compound LaFeAsO is a normal semi-metal which shows a Fermi surface nesting or spin Peierls instability below 150 K with a tetragonal to orthorhombic structural transition, accompanied by a spin density wave (SDW) type antiferromagnetic order [6]. Electron doping to the FeAs layer through F^- -substitution in the O^{2-} site or O^{2-} -deficiency suppresses both the magnetic order and the structural distortion in favor of superconductivity [1, 3]. On the other hand, hole doping through Sr^{2+} -substitution in the R^{3+} site gives similar effect [4]. Therefore, like the high- T_c cuprate systems, the superconductivity in these iron-based compounds occurs in close proximity to a long range antiferromagnetic ground state.

Since the FeAs layer is believed to be the superconducting layer of the $\text{RFeAsO}_{1-x}\text{F}_x$ system, studies on the anisotropic properties are crucial for understanding this new iron-based system. High-quality single crystal is essential for detailed in-depth studies [9, 12]. However, the anisotropic superconducting properties can be easily obtained using a much simpler way. In this report, we use the field-rotation alignment method to align the $T_c = 52$ K $\text{Sm}_{0.95}\text{La}_{0.05}\text{FeAsO}_{0.85}\text{F}_{0.15}$ microcrystalline powder at room temperature. The polycrystalline $\text{Sm}_{0.95}\text{La}_{0.05}\text{FeAsO}_{0.85}\text{F}_{0.15}$ was prepared by con-

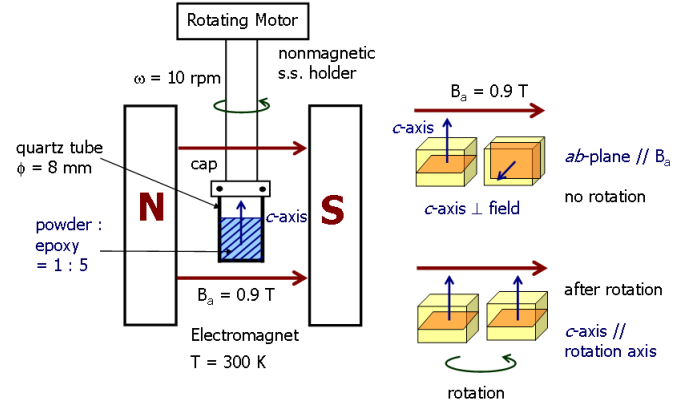


FIG. 1: Block diagram for field-rotation powder alignment method with ab -plane along the aligned magnetic field B_a and c -axis along the rotation axis.

ventional solid state reaction. First the SmAs powder was prepared by reacting Sm and As powders at 650°C for about 5 hours, and fine powders of SmAs , FeAs , Fe , LaF_3 , Fe_2O_3 were mixed together according to the stoichiometric ratio of $\text{Sm}_{0.95}\text{La}_{0.05}\text{FeAsO}_{0.85}\text{F}_{0.15}$, ground thoroughly, and then pressed into pellets. The pellets were wrapped in Ta foil to be sealed in an evacuated quartz tube, and annealed at 1160°C for about 50 hours. The $\text{Sm}_{0.95}\text{La}_{0.05}\text{FeAsO}_{0.85}\text{F}_{0.15}$ powders with an average microcrystalline grain size of $1\text{--}10\ \mu\text{m}$ were mixed with epoxy (4-hour curing time) in a quartz tube ($\phi = 8$ mm) with a powder:epoxy ratio of 1:5. The quartz tube was immediately placed in a 0.9-T electromagnet and rotated at a speed of 10 rpm with the rotation axis perpendicular to the aligned magnetic field B_a (Fig. 1). Since the tetragonal ab -plane of $\text{Sm}_{0.95}\text{La}_{0.05}\text{FeAsO}_{0.85}\text{F}_{0.15}$ microcrystalline is aligned along B_a from X-ray diffrac-

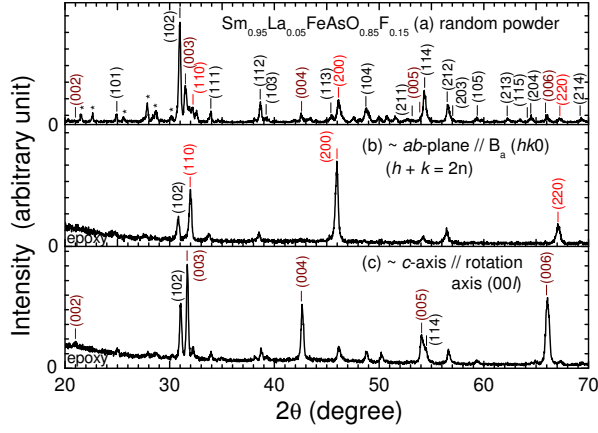


FIG. 2: Powder X-ray diffraction patterns for $\text{Sm}_{0.95}\text{La}_{0.05}\text{FeAsO}_{0.85}\text{F}_{0.15}$. (a) random powder, (b) *ab*-plane aligned along B_a , (c) *c*-axis aligned along rotation axis ($\perp B_a$).

tion study, the rotation perpendicular to B_a will force the microcrystalline *c*-axis to align along the rotation axis.

The X-ray diffraction patterns for $\text{Sm}_{0.95}\text{La}_{0.05}\text{FeAsO}_{0.85}\text{F}_{0.15}$ random powder, partially *ab*-plane aligned along B_a , and partially *c*-axis aligned along the rotation axis are shown collectively in Fig. 2. The unaligned random powder diffraction pattern gives a slightly larger tetragonal lattice parameters of $a = 0.3936(3)$ nm and $c = 0.8495(8)$ nm with 5% La doping than $\text{SmFeAsO}_{0.85}\text{F}_{0.15}$ [5]. At least 10% impurities were observed as marked by asterisk in the diffraction pattern. For *ab*-plane aligned along B_a , enhanced $(hk0)$ diffraction lines ($h + k = 2n$) were observed. The lack of forbidden line (210) is consistent with the space group $P4/nmm$. For *c*-axis aligned along the rotation axis, enhanced $(00l)$ diffraction lines were observed. The imperfect alignment (80-90 %) with the appearance of major (102) line may be due to intrinsic weak magnetic anisotropy, low aligned field (0.9 T), imperfect powder preparation or alignment procedure. The diffraction pattern for nonsuperconducting $\text{SmFeAsO}_{0.95}\text{F}_{0.05}$ aligned powder gives similar result with *ab*-plane aligned along B_a .

The field-rotation alignment method at room temperature is based on magnetic anisotropy due to the spin-orbital related anisotropic exchange coupling. There are two major contributions of magnetic moment at room temperature $\chi \sim \chi(\text{Fe}) + \chi(\text{Sm})$. The large Sm^{3+} ($4f^5 5s^2 5p^6$, $S = 5/2$, $L = 5$, $J = L - S = 5/2$) localized moment in the insulating $(\text{Sm}_{0.95}\text{La}_{0.05})(\text{O}_{0.85}\text{F}_{0.15})$ layer has weak anisotropic exchange coupling. On the other hand, the Fe^{2+} ($3d^6$) itinerant moment in the metallic FeAs layer is rather small from powder neutron diffraction data and band structure calculation. The Fe^{2+} feels the distorted FeAs_4 tetrahedral crystal field with three low-lying manifold and two up-lying manifold (d_{xz}

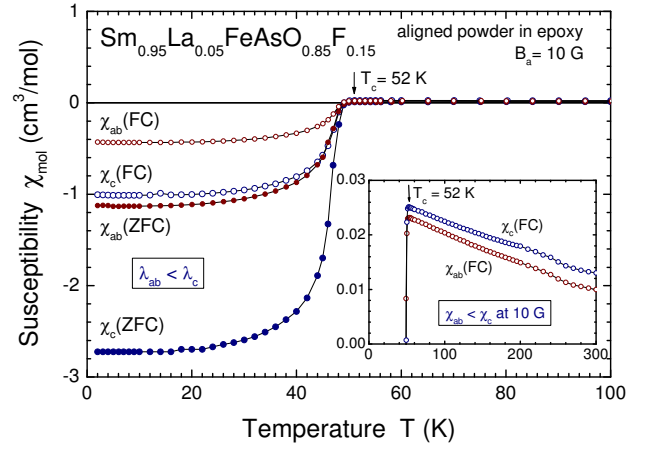


FIG. 3: Anisotropic low-field FC and ZFC susceptibility $\chi_{ab}(T)$ and $\chi_c(T)$ for aligned $\text{Sm}_{0.95}\text{La}_{0.05}\text{FeAsO}_{0.85}\text{F}_{0.15}$.

and d_{yz}). The six $3d$ electrons are distributed in three quasi-2D hole-like bands and two electron-like bands with Fermi surfaces from five $3d$ orbitals. Anisotropic exchange coupling (magnetic fluctuation) occurs from strong Fe-As $3d_{xz,yz}$ -4p hybridization and Fe-Fe $3d_{xy}$ - $3d_{xy}$ direct electron hopping between neighboring Fe atoms in the tetragonal basal *ab*-plane [6, 10, 11]. In the aligned magnetic field, anisotropic Fe orbitals are tied to the spin direction, and a strong spin-orbital related anisotropic exchange coupling at 300 K should dominate the magnetic alignment. Due to the quasi-2D FeAs layer structure, anisotropic Fe magnetic susceptibility $\chi_{ab}(\text{Fe}) > \chi_c(\text{Fe})$ is expected to be the dominant factor for *ab*-plane alignment along B_a at 300 K. Indeed, anisotropic room temperature magnetization for $\text{Sm}_{0.95}\text{La}_{0.05}\text{FeAsO}_{0.85}\text{F}_{0.15}$ aligned powder was observed with weak magnetic anisotropy ratio $\chi_{ab}/\chi_c \sim 1.2$ up to 7 T. In the low field region, a cross-over from $\chi_c \geq \chi_{ab}$ to $\chi_c \leq \chi_{ab}$ at high field with nonlinear behavior may be caused by the magnetic impurities.

Magnetization and magnetic susceptibility data were collected with a Quantum Design 1-T μ -metal shielded MPMS₂ or a 7-T MPMS superconducting quantum interference device (SQUID) magnetometer from 2 K to 300 K. The anisotropic temperature dependence of molar magnetic susceptibility $\chi_{ab}(T)$ and $\chi_c(T)$ for aligned powder $\text{Sm}_{0.95}\text{La}_{0.05}\text{FeAsO}_{0.85}\text{F}_{0.15}$ with applied field along the *ab*-plane and *c*-axis are shown collectively in Fig. 3. For aligned dispersed microcrystalline in low applied field of 10 G, both zero-field-cooled (ZFC) and field-cooled (FC) data revealed a sharp superconducting transition temperature T_c of 52 K, which is identical to the measured T_c from bulk polycrystalline sample. Large ZFC intragrain Meissner shielding signals were observed with an almost constant $\chi_c = -2.72$ cm³/mol and $\chi_{ab} = -1.13$ cm³/mol up to 20 K. The anisotropic diamagnetic parameter $\gamma = \chi_c/\chi_{ab}$ of 2.4 was deduced for aligned mi-

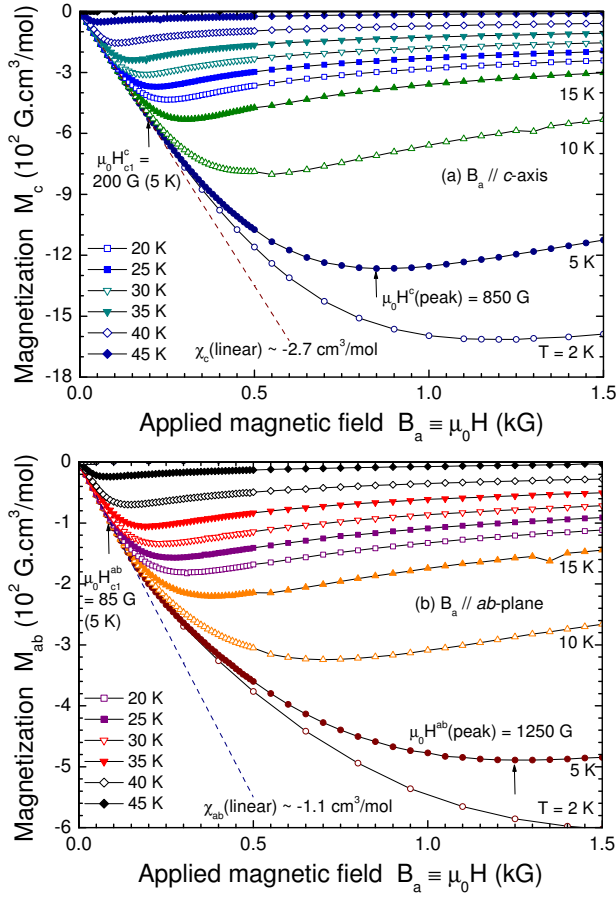


FIG. 4: Temperature variation of (a) c -axis superconducting initial magnetization $M_c(B_a)$ and (b) ab -plane superconducting initial magnetization $M_{ab}(B_a)$ for aligned $\text{Sm}_{0.95}\text{La}_{0.05}\text{FeAsO}_{0.85}\text{F}_{0.15}$ powder.

microcrystalline. The FC flux-trapped signal gave the same anisotropic parameter γ of 2.4. Considering the imperfect alignment factor (80-90%), a larger anisotropic diamagnetic parameter $\gamma = 2.4 \pm 0.6$ was derived. For temperature above T_c , normal state paramagnetic anisotropy ratio χ_c/χ_{ab} of 1.3 was observed in 10 G at 300 K, which is consistent with low field magnetization at 300 K and may be caused by magnetic impurities. No trace of Curie-Weiss-like behavior was observed in the normal state.

The temperature variation of superconducting initial magnetization curves with applied field B_a along c -axis, $M_c(B_a, T)$, and ab -plane, $M_{ab}(B_a, T)$, for aligned $\text{Sm}_{0.95}\text{La}_{0.05}\text{FeAsO}_{0.85}\text{F}_{0.15}$ powder from 2 K to 45 K are shown in Fig. 4(a) and 4(b), respectively. For example, at $T = 5$ K, the maximum diamagnetic signal was observed at magnetization peak field $\mu_0 H^c(\text{peak})$ of 850 G for M_c and a larger $\mu_0 H^{ab}(\text{peak})$ of 1250 G for M_{ab} , indicating anisotropic pinning for different applied field directions. The peak field corresponds to the field that magnetic flux penetrates into the center of aligned superconducting microcrystallines forming a vortex glass

where vortex are mainly pinned by impurities and imperfections. At the low-field region, linear variation of magnetization as an evidence of Meissner state was clearly observed for both directions [13]. The low-field linear slopes of initial magnetization are consistent with the low-field ($B_a = 10$ G) susceptibility as measured in Fig. 3. Since the lower critical field $\mu_0 H_{c1}$ is the field flux start to penetrate into the superconductor forming mixed state, the magnetization $M(B_a)$ deviates from the linear response of Meissner state. Using 10-G/5-K linear magnetic susceptibility $\chi_c = -2.7 \text{ cm}^3/\text{mol}$ and $\chi_{ab} = -1.1 \text{ cm}^3/\text{mol}$ in Fig. 3, lower critical field $\mu_0 H_{c1}^c$ of 200 G and $\mu_0 H_{c1}^{ab}$ of 85 G were deduced from the linear susceptibility extrapolation lines.

The low temperature, low magnetic field anisotropic phase diagram for aligned $\text{Sm}_{0.95}\text{La}_{0.05}\text{FeAsO}_{0.85}\text{F}_{0.15}$ powder is shown in Fig. 5(a). The zero temperature lower critical field $\mu_0 H_{c1}^c(0)$ of 230 G and $\mu_0 H_{c1}^{ab}(0)$ of 95 G were extrapolated. The temperature dependence of anisotropic penetration depth $\lambda_{ab}(T)$ and $\lambda_c(T)$ are shown in Fig. 5(b), using the anisotropic formula $\mu_0 H_{c1}^c = \Phi_0/2\pi\lambda_{ab}^2$ and $\mu_0 H_{c1}^{ab} = \Phi_0/2\pi\lambda_{ab}\lambda_c$, where Φ_0 is the flux quantum. The zero temperature penetration depths $\lambda_c(0) = 280$ nm and $\lambda_{ab}(0) = 120$ nm were extrapolated. These values reflect the quasi-2D FeAs layer structure and are smaller than the microcrystalline grain size of ~ 1 -10 μm . The anisotropy parameter γ derived from the penetration depth ratio $\lambda_c(0)/\lambda_{ab}(0)$ of 2.33 is smaller than the reported value from single crystal by penetration depth (~ 4) [12] or $\mu_0 H_{c2}$ (~ 4.34 -4.9) [9]. However, the differences of anisotropy parameter γ may be attributed to the different demagnetization field in slab-shaped single crystal with different applied field directions when the geometric shape is considered, i.e. the slab shape of single crystals and the sphere-like shape of the aligned microcrystalline in this work.

Since the band structure calculations suggested quasi-2D nature of the Fermi surface [10, 11] in the layered Fe-based compounds, the ab -plane penetration depth behavior was expected to provide more intrinsic information than c -axis. The low temperature (2-25 K) penetration depth $\lambda_{ab}(T)$ can be roughly fitted by a BCS-type s-wave exponential law [12]

$$\frac{\lambda_{ab}(T) - \lambda_{ab}(0)}{\lambda_{ab}(0)} = \sqrt{\frac{\pi\Delta_0}{2T}} \exp\left(-\frac{\Delta_0}{k_B T}\right). \quad (1)$$

but with a much smaller $\Delta_0/k_B T_c$ of 0.4 than typical value of 1.76, indicating that isotropic s-wave model may not be a good one for this new high- T_c superconductor, although a BCS-like gap is reported for $\text{SmFeAsO}_{0.85}\text{F}_{0.15}$ from Andreev spectra [7]. However, the low temperature $\lambda_{ab}(T)$ can also be well fitted with a simple linear- T dependence, indicating existence of nodal quasiparticle excitation, possibly d-wave or extended s-wave pairing in nature [11]. A triplet p-wave pairing

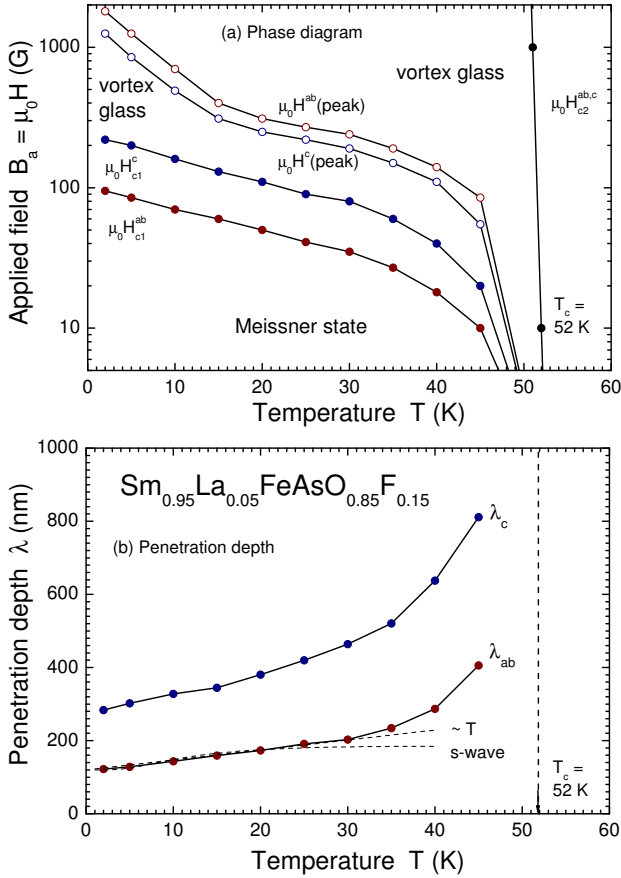


FIG. 5: (a) Low field anisotropic phase diagram $\mu_0 H(T)$ for aligned $\text{Sm}_{0.95}\text{La}_{0.05}\text{FeAsO}_{0.85}\text{F}_{0.15}$ powder. (b) Temperature dependence of anisotropic penetration depth $\lambda_{ab}(T)$ and $\lambda_c(T)$.

model with strong ferromagnetic fluctuation and degenerate electron Fermi surfaces was also proposed from band structure consideration [10]. In the powder alignment procedure, Fe spin-orbital-related anisotropic magnetic fluctuation is needed at 300 K. However, we can not distinguish whether the magnetic fluctuation is ferromagnetic or antiferromagnetic in origin.

The anisotropic high-field (± 7 T) isothermal superconducting hysteresis loops M - B_a at 5 K (Fig. 6) indicate that upper critical field $\mu_0 H_{c2}$ in both directions are much larger than maximum applied field of 7 T with very short anisotropic coherence lengths ξ_{ab} and ξ_c . Moreover, hysteresis loops with large paramagnetic background indicate the large magnetic/impurity contribution.

In conclusion, due to Fe spin-orbital-related short-range anisotropic exchange interaction $\chi_{ab}(\text{Fe}) > \chi_c(\text{Fe})$ at 300 K, $\text{Sm}_{0.95}\text{La}_{0.05}\text{FeAsO}_{0.85}\text{F}_{0.15}$ microcrystalline powder can be aligned using the field-rotation alignment method where ab -plane is parallel to the aligned field B_a and c -axis is parallel to the rotation axis. Rather small superconducting anisotropy parameter $\gamma \sim 2.4 + 0.6$ was observed (from both susceptibility and lower crit-

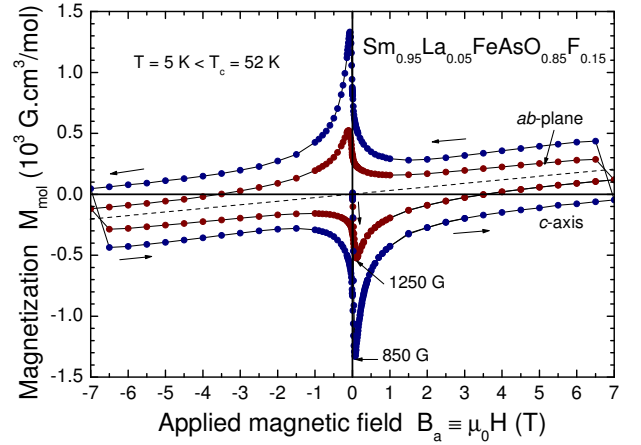


FIG. 6: Anisotropic high-field superconducting hysteresis loop $M_c(B_a)$ and $M_{ab}(B_a)$ at 5 K for aligned $\text{Sm}_{0.95}\text{La}_{0.05}\text{FeAsO}_{0.85}\text{F}_{0.15}$ powder.

ical field). The magnetic fluctuation used for powder alignment at 300 K may be related with the pairing mechanism of superconductivity at lower temperature.

This work was supported by NSC95-2112-M-007-056-MY3, NSC97-2112-M-003-001-MY3, NSFC50421201, MSTC2006CB601003, and MSTC2006CB922005.

* Electronic address: hcku@phys.nthu.edu.tw

- [1] Y. Kamihara, T. Watanabe, M. Hirano, and H. Hosono, *J. Am. Chem. Soc.* **130**, 3296 (2008).
- [2] H. Takahashi, K. Igawa, K. Arii, Y. Kamihara, M. Hirano, and H. Hosono, *Nature* **453**, 376 (2008).
- [3] T. A. Ren, G. C. Che, X. L. Dong, J. Yang, W. Lu, W. Yi, X. L. Shen, Z. C. Li, L. L. Sun, F. Zhou, and Z. X. Zhao, *Europhys. Lett.* **83**, 17002 (2008).
- [4] H. H. Wen, G. Mu, L. Fang, H. Yang, and X. Zhu, *Europhys. Lett.* **83**, 17009 (2008).
- [5] X. H. Chen, T. Wu, G. Wu, R. H. Liu, H. Chen, and D. F. Fang, *Nature* **453**, 761 (2008).
- [6] C. de la Cruz, Q. Huang, J. W. Lynn, J. Y. Li, W. Ratcliff II, J. L. Zarestky, H. A. Mook, G. F. Chen, J. L. Luo, N. L. Wang, P. C. Dai, *Nature* **453**, 899 (2008).
- [7] T. Y. Chen, Z. Tesanovic, R. H. Liu, X. H. Chen, and C. L. Chien, *Nature* **453**, 1224 (2008).
- [8] G. F. Chen, Z. Li, D. Wu, G. Li, W. Z. Hu, J. Dong, P. Zheng, J. L. Luo, and N. L. Wang, *Phys. Rev. Lett.* **100**, 247002 (2008).
- [9] Y. Jia, P. Cheng, L. Fang, H. Q. Luo, H. Yang, C. Ren, L. Shan, C. Z. Gu, and H. H. Wen, *arXiv:cond-mat/0806.0532* (2008).
- [10] G. Xu, W. Ming, Y. Yao, X. Dai, S. C. Zhang, and Z. Fang, *Europhys. Lett.* **82**, 67002 (2008).
- [11] X. Dai, Z. Fang, Y. Zhou, and F. C. Zhang, *arXiv:cond-mat/0803.3982* (2008).
- [12] C. Martin, R. T. Gordon, M. A. Tanatar, M. D. VanNette, M. E. Tillman, E. D. Mun, P. C. Canfield, V. G. Kogan, G. D. Samolyuk, J. Schmalian, and R. Prozorov,

- arXiv:cond-mat/0807.0876v1 (2008).
- [13] X. G. Li, X. F. Sun, Y. H. Toh, Y. Y. Hsu, and H. C. Ku, Phys. Rev. B **58**, 1000 (1998).